Imaging subwavelength holes using an apertureless near-field scanning optical microscope

F. Formanek,[a] Y. De Wilde, and L. Aigouy
Laboratoire d'Optique Physique, CNRS UPR A0005, École Supérieure de Physique et de Chimie Industrielles, 10 rue Vauquelin, 75005 Paris, France

(Received 3 December 2002; accepted 20 March 2003)

We present investigations of the light scattered by subwavelength holes in a chromium film using an apertureless near-field scanning optical microscope, which operates either in the visible ($\lambda = 655$ nm) or in the infrared ($\lambda = 10.6\ \mu$m). The near-field optical images exhibit patterns around the holes that seem to coincide with the component of the stray electrical field parallel to the tip axis. A tip–sample dipole coupling model provides a satisfactory description of the experimental data recorded in the infrared with light polarized normally to the sample surface. © *2003 American Institute of Physics.* [DOI: 10.1063/1.1574178]

I. INTRODUCTION

The principle of near-field scanning optical microscopes (NSOMs) is to bring a nanometer probe very close to the surface of an illuminated sample in order to locally reveal the evanescent field confined at the surface and to achieve subwavelength resolution. The most widespread NSOMs use tapered metal-coated optical fibers with a subwavelength aperture as either a light source[1] or a light collector.[2] The resolution, determined by the aperture size, is limited in this case to about 50–100 nm. A more recent kind of NSOM, called ANSOM for apertureless near-field scanning optical microscope, uses a sharp metallic tip to scatter the optical near-field generated by an external illumination and to convert it into a radiating field.[3] This propagative field can then be detected in the far-field by a classical optical detector. This system can operate at any wavelength and generally achieves a somewhat higher resolution than fiberoptic NSOMs, given by the radius of curvature of the tip apex, independently of the wavelength.[4]

Well-defined test samples with subwavelength structures are required to get a better insight into what is actually detected in a near-field optical microscope. These can be, for instance, sharp metallic steps on a dielectric substrate,[5] subwavelength holes and islands of various shape and nature,[6,7] or even individual fluorescent molecules.[8,9] Another subject of interest is the field transmitted through arrays of subwavelength holes regularly displayed in a metallic screen.[10,11] Experiments on these systems reveal extraordinary transmission at well-defined wavelengths in the far-field.[10] In addition to this far-field property, theory predicts the presence of lobes in the near-field distribution around each of these coupled holes[11] or even individual holes.[9]

This article deals with a near-field optical study performed with an ANSOM in the visible and in the infrared on a test sample,[12] which consists of circular subwavelength holes randomly distributed in metallic thin films. The optical images reveal important variations of the near-field signal in the vicinity of the holes, which we ascribe to stray fields. In addition to the recording of high resolution optical images of the subwavelength holes, we have investigated in detail the dependence of the near-field signal in the infrared as a function of the tip-sample separation by performing tip retract curves. The results of this study are compared with the prediction of a simple model in which the tip is described as a dipole interacting with its image in the sample.[13]

II. EXPERIMENTAL SETUP

Our homemade ANSOM operates either with a visible or with an infrared illumination.[14] A schematic view of the experimental setup is presented in Fig. 1. For this experiment, we use sharp tungsten tips prepared by electrochemical etching. The tip, which is glued onto a tuning fork, oscillates vertically in tapping mode and periodically scatters the evanescent field towards an optical detector. A lock-in amplifier placed in series with the detector extracts the near-field contribution from the far-field background, while the topography of the sample is simultaneously recorded. The setup is built around a commercial optical microscope, with a large numerical aperture (NA) objective lens. The microscope is positioned so that the apex of the tip, which is in contact with the sample surface, is in the focal plane of the objective. For the measurements in the visible, a laser diode ($\lambda = 655$ nm) delivering a few tens of milliwatts is focused through the microscope objective ($50\times$, NA$=0.6$) on the tip apex, producing a spot of about 1-μm diameter on the surface. The polarization of the beam which enters the objective can be tuned at the diode exit. The field scattered by the tip, as well as the reflected beam, are then collected by the same objective in reflection mode and directed towards a silicon diode. For the measurements in the infrared, we use a CO_2 laser ($\lambda \simeq 10.6\ \mu$m) focused at grazing incidence on the tip via a ZnSe lens with a 10-cm focal distance. In this experiment, the polarization of the incident beam is quasinormal to the sample surface. The scattered light is collected by a Casseg-

[a]Electronic mail: formanek@optique.espci.fr

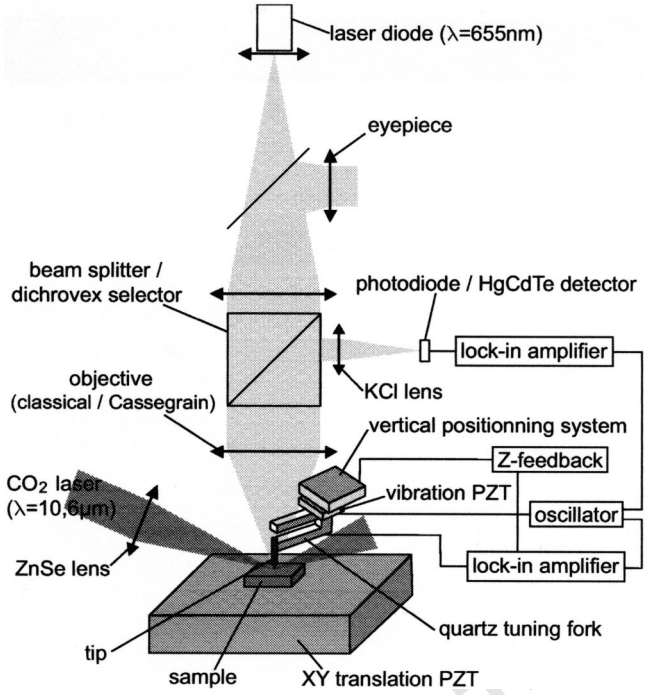

FIG. 1. Schematic view of both visible and infrared experimental setups.

rain objective (36×, NA=0.5) made up of two gold spherical mirrors, before being sent to a nitrogen-cooled HgCdTe detector.

III. RESULTS

The studied sample is made of small circular holes randomly distributed over a thin chromium layer evaporated on a glass substrate.[12] These structures show a simple crater-like geometry as seen on the topographic images [Figs. 2(a) and 2(c)]. On Fig. 2(a), the holes appear almost circular, with an outer diameter of about 370 nm and an inner diameter close to 250 nm. The slight ellipticity is due to thermal drift during the scan. The bottom of the holes, made of glass, looks dark, whereas some features (probably dust) situated above the surface appear lighter than the chromium. Each hole's depth is estimated from a cross section cut to 25 nm.

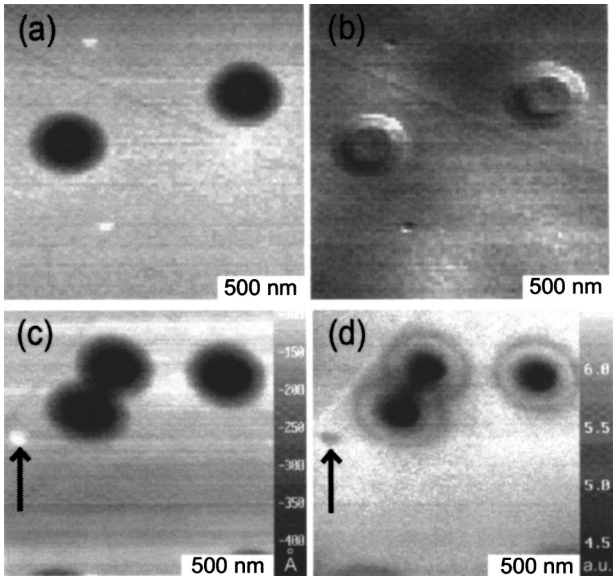

FIG. 2. (a) Topographic image. (b) Near-field image (λ=655 nm). (c) Topographic image. (d) Near-field image (λ=10.6 μm).

The optical images recorded in the visible [Fig. 2(b), λ=655 nm] show mostly two optical lobes of opposite contrast on both sides of the holes. The amplitude of the dark (respectively, the light) lobe is lower (respectively, greater) than the signal inside the hole. The optical resolution of the ANSOM is estimated to about 20 nm from the full width at half-maximum of the smallest details that can be reproducibly imaged.

Figure 2(d) is an optical near-field image taken at λ≃10.6 μm with a laser power of 70 mW in another part of the sample, corresponding to the topographic image shown in Fig. 2(c). In this case, the optical signal is depleted in the center of the holes. In addition, each hole is surrounded by a dark ring; this local minimum of the optical signal coincides with the outer diameter of the hole (i.e., the upper edge of the crater) seen in topography. The symmetry of this feature is likely related to the normal polarization of the incoming light, which does not break the circular symmetry of the holes. The optical spatial resolution is nearly the same as that in the visible images: ~30 nm, depending only on the radius of curvature of the tip apex. One can also note the presence of a small ''dust'' on the surface, appearing as a bright structure in the topographic image [indicated by the arrow on Fig. 2(c)], revealing a small bump on the chromium surface. The optical signal on this bump in Fig. 2(d) is somewhat lower than that obtained on the chromium regions. This dust is probably an organic particle from the environment or a small piece of polymer remaining on the surface after the sample preparation, which results in a locally enhanced cross-section extinction compared to chromium.[4,15] This results demonstrates that the optical contrast in the near-field images is due to local variation of the optical properties of the material under the tip and not to a bad electronic feedback on the tip positioning. This also illustrates the power of the ANSOM to discriminate different materials on nanometer scale, which is not feasible with an atomic force microscope (AFM).[15,16]

Besides imaging, we have also studied the dependence of the near-field signal as a function of the distance between the tip and the chromium film; this study was performed in the infrared. In this case, the lateral illumination with a vertically polarized laser beam guarantees a polarization parallel to the tip axis. In these experiments, the infrared signal was demodulated by the lock-in at either the tuning fork dither frequency ω ($\simeq$15 kHz), or its higher harmonics 2ω and 3ω. The feedback loop is turned off while the tip is slowly retracted away from the sample surface. Figure 3(a) presents the experimental results of these ''retract'' curves with a free oscillation amplitude of the tip estimated at 75 nm. All the curves start at the contact point (probe–sample distance =0) and are normalized to unity. A strong enhancement of the infrared signal is observed at short distance. The 2ω and 3ω curves almost vanish beyond 50 nm, while the ω signal shows a slower decay. Compared to other setups,[13] the tip of our ANSOM covers a total vertical range of about 18 μm.

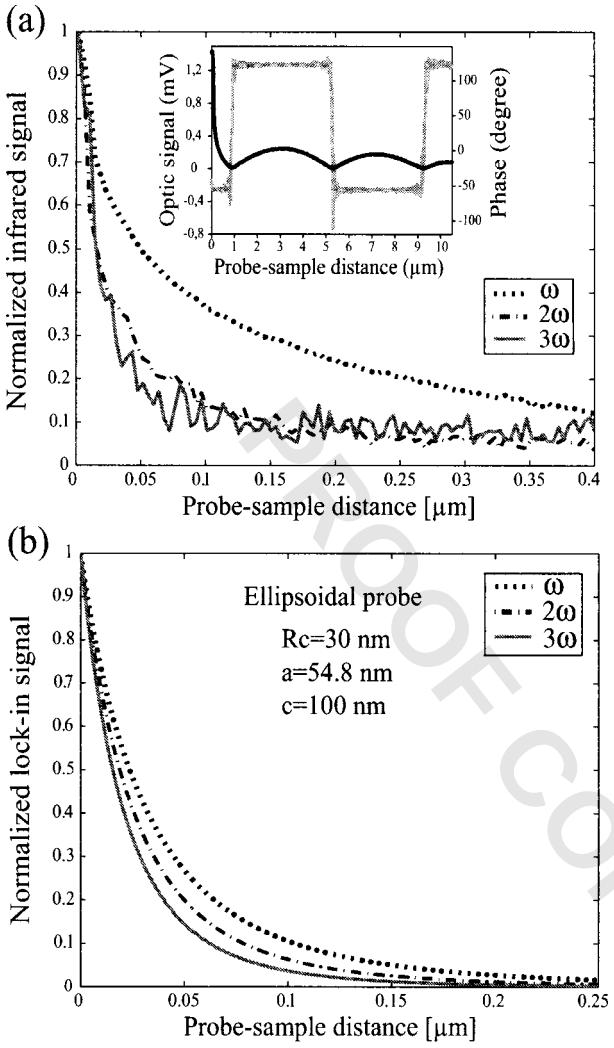

FIG. 3. (a) Experimental retract curves measured at $\lambda = 10.6\ \mu$m. Inset: large-scale retract curve at ω. (b) Calculated approach curves for an ellipsoidal tip with $R_c = 30$ nm.

Hence, the optical signal can be investigated over distances larger than the wavelength even in the infrared. Over such large distances, the optical signal at ω exhibits oscillations [Fig. 3(a) inset]. In contrast, no oscillations were observed in the optical signal at 2ω and 3ω.

IV. DISCUSSION

Let us now try to interpret these experimental results. Near-field images with antisymmetric lobes at the edges of the holes [Fig. 2(b)] have been reproducibly observed whenever the incident laser beam is polarized parallel to the film. This feature has been seen with several tips in our ANSOM, which operates in reflection mode at 655 nm. It has also been confirmed with two other experimental setups[5,17] which operates in reflection or in transmission mode at various wavelengths between 600 nm and 1 μm. The absence of correlation between the scan direction and the orientation of the lobes, as well as the observation of the lobes on a flat background and at higher harmonics, rule out the possibility of an experimental artifact. A verification of the purely optical origin of the effect was also obtained in constant height mode,

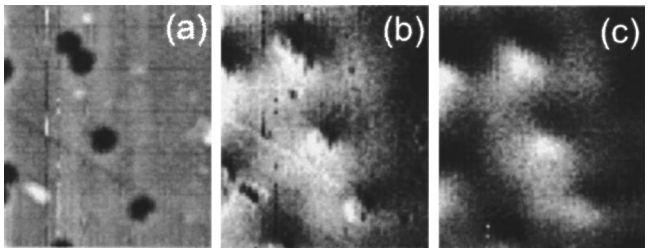

FIG. 4. Images obtained with a transmission mode ANSOM ($\lambda = 780$ nm, scan size: 2.5 μm$\times$3 μm). (a) Topographic image, (b) optical images recorded in tapping mode, that is, with the feedback loop active; and (c) in constant height mode, with the feedback loop disconnected and the tip slightly withdrawn.

that is, without the feedback loop active, as shown in Fig. 4(c). This mode requires one to withdraw the tip a few tens of nanometers away from the sample surface in order to prevent tip damages during the scans. As expected, this results in blurred optical images compared to the situation where the tip is closer and hits the surface intermittently [see Fig. 4(b)]; despite this loss of resolution, one can still distinguish antisymmetrical lobes around each hole.

We are currently not able to establish a clear correlation between the polarization of the incident beam and the orientation of the lobes. In fact, in the experimental configuration used for the visible illumination, we can only control the polarization direction at the exit of the laser diode. However, with a linearly polarized incident beam, the polarization components in the focal plane of our large numerical aperture objective exhibit significant spatial variations.[18] The focal spot is also strongly disturbed due to light scattering and shadowing effects by the upper parts of the tip cone and the tip mounting (Fig. 1), and the tip geometry may itself influence the polarization. A precise control of the polarization in the vicinity of the tip apex would require a very well-defined illumination and a fine positioning mechanism of the tip within the focal spot[19] (less than 1 μm in our case), which is not available at this stage in our setup.

Yet, the data suggest that the antisymmetric lobes result from an antisymmetrical distribution of surface charges induced by a component of the electric field parallel to the chromium film,[9,11,17,20] producing a stray field with off-plane components around the hole, as schematically shown on Fig. 5. Within this scenario, the z component of the electric stray

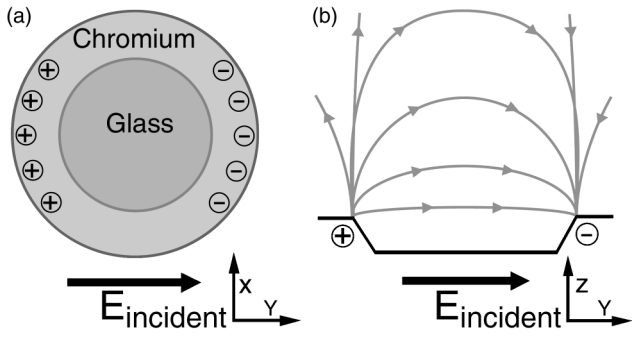

FIG. 5. (a) Distribution of surface charges around a hole under illumination. (b) Resulting stray field distribution.

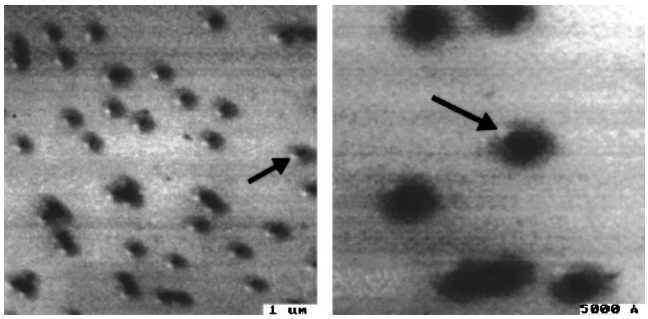

FIG. 6. Optical images recorded in the infrared with two different tips ($\lambda = 10.6\ \mu$m, normal polarization). A bright spot is observed around each hole at a well-defined orientation indicated by the arrows.

field E_z, would exhibit lobes of opposite signs, similar to our experimental results [Fig. 2(b)]. Hence, the tip seems to be more sensitive to the z component of the electric stray field, rather than to in-plane components. Interestingly, we note that the experimental observation of antisymmetric lobes [Fig. 2(b)] indicates that the information related to the phase of the scattered field is preserved in our detection. This is due to interference effects between the field scattered by the tip and a background field scattered by the sample surface, leading to homodyne detection.[13] In addition, these interference effects are confirmed by the observation of oscillations, including phase shifts of 180°, on the scale of λ in the visible and in the infrared [Fig. 3(a) inset] on these metallic films. The interference effects, which are observed here in the infrared, also indicate that the ANSOM is mainly sensitive to the amplitude of the field scattered by the tip, and not to its intensity. The resulting oscillations, which perturb the signal at ω at short probe–sample distance, can significantly be suppressed when demodulating the signal at higher harmonics (2ω, $3\omega, \ldots$), as already reported.[13] Note that while most near-field optical images performed in the infrared exhibit a circular symmetry around each hole, we occasionally also observed images such as that presented in Fig. 6 with a bright spot at a well-defined orientation, suggesting that, in some cases, a defect or a tilt at the tip apex breaks the circular symmetry of the field that is scattered around the holes. A systematic investigation of the near-field signal as a function of the polarization of the incident light and the tip geometry is planned in order to shed light on the influence of these parameters on the near-field optical images.

The optical contrast R_{exp}, defined as the ratio between the lock-in signal at ω in the center of the holes (made of glass) and on the chromium surface is about 0.7 in the experimental infrared images. We use a modified version of Mie's theory, which takes into account the interaction of the probe dipole with its electrostatic image[13] to calculate the scattering cross section C_{sca} in the infrared of the tungsten tip (optical index $n_W = 10 + 45i$) on a chromium ($n_{\mathrm{Cr}} = 13 + 27i$) or glass ($n_{\mathrm{glass}} = 2.694 + 0.509i$) sample, with the electric field oriented normally to the surface. Based on this dipole model, we can evaluate a theoretical contrast R_{th}, taking into account the periodical modulation of the tip–sample distance. Assuming a spherical tip of radius 30 nm, based on our lateral resolution, and a dither amplitude of the tip of 70 nm, we find $R_{\mathrm{th}} = 0.66$, in good agreement with our experimental results. However, we must assume a much larger tip radius within the same dipole model, in the range of 150 nm, to be able to fit in a satisfactory way the retract curves shown in Fig. 3(a). Such a large tip radius is, of course, not reasonable in view of the high lateral resolution of our probe. This contradiction can be resolved if one uses an extended Mie's theory for elliptical particles to depict the tip. We consider an ellipsoidal tip[21] with a semimajor axis c (along the z direction) and a semiminor axis $a < c$. The polarizability of such an ellipsoid along the z axis is given by

$$\alpha = 4\pi a^2 c \left[\frac{\epsilon - 1}{3 + 3A(\epsilon - 1)} \right], \tag{1}$$

where ϵ is the tip dielectric constant and A is a depolarization factor[22] related to the shape of the tip. One must replace in the dipole model the probe by a point dipole located at a distance R_c above the tip apex,[21] where $R_c = a^2/c$ is the tip's radius of curvature. Assuming $R_c = 30$ nm with $c = 100$ nm and $a = 54.8$ nm, we obtain $A = 0.1913$ ($A = 1/3$ for a sphere). Figure 3(b) shows the calculated $\sqrt{C_{\mathrm{sca}}}$ (proportional to the amplitude of the scattered field) demodulated at ω, 2ω, and 3ω as a function of the tip–sample distance, assuming a dither amplitude of 70 nm. A satisfactory agreement for the curves at 2ω and 3ω is found between theory [Fig. 3(b)] and experiment [Fig. 3(a)]. The experimental curve recorded at ω [Fig. 3(a)] exhibits a much slower decay at short distances than theoretically predicted, due to the interference term which is superimposed on the signal [Fig. 3(a) inset].

The ω-signal measured while in contact with the surface is of the order of 60 nW for an incident laser power of 50 mW. Regarding to Mie's theory, we expect the unmodulated signal scattered towards the detector to be around 10 fW for a spherical tip of radius 30 nm, and around 4 pW for an ellipsoidal tip as described earlier. The corresponding signals demodulated by the lock-in at ω would then be about 1 fW and 0.2 pW, respectively. The optical signal that is measured experimentally is significantly higher than the theoretical predictions, due to the high antenna gain of the tip.[13] Note that the optical contrast between the glass and the chromium remains almost unchanged, despite the use of an elliptical shape for the tip instead of a spherical shape.

V. CONCLUSION

In conclusion, we have achieved high-resolution optical images of subwavelength holes in the visible and in the infrared. Our results suggest that the tip mainly reveals the z component of the electric field, rather than its intensity, due to homodyne detection. The antisymmetric lobes observed in the visible may qualitatively be explained by the presence of stray fields resulting from an asymmetric distribution of surface charges around the holes. Finally, an extended version of the dipole model, which describes the tip as an elongated ellipsoid, instead of as a sphere, gives good results to describe at the same time the dependence of the near-field signal as a function of the tip–sample separation, the optical contrast from one material to another, and the spatial resolution of the near-field images.

ACKNOWLEDGMENTS

The authors wish to thank H. Cory and A. C. Bocarra for stimulating discussions, and C. Bainier and D. Courjon (Université de Franche-Compté) for providing the samples within the GDR ''Optique du Champ Proche.'' Part of this work (Y. D. W., F. F.) has been funded by the French Ministère de la Recherche, ACI Jeunes Chercheurs, project number 2039.

[1] E. Betzig and J. Trautman, Science (Washington, DC, U.S.) **257**, 189 (1992).
[2] E. Betzig, M. Isaacson, and A. Lewis, Appl. Phys. Lett. **51**, 2088 (1987).
[3] F. Zenhausern, M. O'Boyle, and H. Wickramasinghe, Appl. Phys. Lett. **65**, 1623 (1994).
[4] B. Knoll and F. Keilmann, Nature (London) **399**, 134 (1999).
[5] R. Bachelot, P. Gleyzes, and A. Boccara, Opt. Lett. **20**, 1924 (1995).
[6] J. Michaelis, C. Hettich, J. Mlynek, and V. Sandoghdar, Nature (London) **405**, 325 (2000).
[7] J. Krenn, A. Dereux, J. Weeber, E. Bourillot, Y. Lacroute, J. Goudonnet, G. Schider, W. Gotschy, A. Leitner, F. Aussenegg, and C. Girard, Phys. Rev. Lett. **82**, 2590 (1999).
[8] C. Hollars and R. Dunn, J. Chem. Phys. **112**, 7822 (2000).
[9] E. Betzig and R. Chichester, Science (Washington, DC, U.S.) **262**, 1422 (1993).
[10] T. Ebbesen, H. Lezec, H. Ghaemi, T. Thio, and P. Wolff, Nature (London) **391**, 667 (1998).
[11] L. Salomon, F. Grillot, A. Zayats, and F. De Fornel, Phys. Rev. Lett. **86**, 1110 (2001).
[12] C. Bainier, C. Vannier, D. Courjon, J.-C. Rivoal, S. Ducourtieux, Y. De Wilde, L. Aigouy, F. Formanek, L. Belliard, P. Siry, and B. Perrin, Appl. Opt. **42**, 691 (2003).
[13] B. Knoll and F. Keilmann, Opt. Commun. **182**, 321 (2000).
[14] Y. De Wilde, F. Formanek, L. Aigouy, W. Kwok, and L. Paulius (unpublished).
[15] R. Hillenbrand and F. Keilmann, Appl. Phys. Lett. **80**, 25 (2002).
[16] R. Hillenbrand, T. Taubner, and F. Keilmann, Nature (London) **418**, 159 (2002).
[17] S. Ducourtieux, Ph.D. thesis, Paris 6 University, 2001.
[18] B. Sick, B. Hecht, U. Wild, and L. Novotny, J. Microsc. **202**, 365 (2001).
[19] A. Bouhelier, M. Beversluis, A. Hartschuh, and L. Novotny, Phys. Rev. Lett. **90**, 013903 (2003).
[20] R. Grober, T. Rutherford, and T. Harris, Appl. Opt. **35**, 3488 (1996).
[21] J. Bohn, D. Nesbitt, and A. Gallagher, J. Opt. Soc. Am. **18**, 2998 (2001).
[22] O. Sqalli, I. Utke, P. Hoffmann, and F. Marquis-Weible, J. Appl. Phys. **92**, 1078 (2002).